Modular [(Fe8M6II)-M-III](&ITn&IT+)(M-II = Pd, Co, Ni, Cu) Coordination Cages

Modular $[Fe^{III}_8M^{II}_6]^{n+}$ (M^{II} = Pd, Co, Ni, Cu) Coordination Cages

S. Sanz,[†]* H. M. O'Connor,[†] P. Comar,[†] A. Baldansuren,[‡] M. B. Pitak,[¶] S. J. Coles,[¶] H. Weihe,[§] N. F. Chilton,[‡] E. J. L. McInnes,[‡] P. J. Lusby,[†]* S. Piligkos[§]* and E. K. Brechin[†]*

[†]EaStCHEM School of Chemistry, University of Edinburgh, David Brewster Road, Edinburgh, EH9 3FJ, UK

[¶]UK National Crystallography Service, Chemistry, University of Southampton, Southampton, Highfield Campus, SO17 1BJ, UK

[§]Department of Chemistry, University of Copenhagen, Universitetsparken 5, DK-2100, Copenhagen, Denmark

[‡]EPSRC National EPR Facility, School of Chemistry and Photon Science Institute, The University of Manchester, Oxford Road, Manchester, M13 9PL, UK

ABSTRACT: Reaction of the simple metalloligand $[Fe^{III}L_3]$ (HL = 1-(4-pyridyl)butane-1,3-dione) with a variety of different M^{II} salts results in the formation of a family of heterometallic cages of formulae $[Fe^{III}_8Pd^{II}_6L_{24}]Cl_{12}$ (**1**), $[Fe^{III}_8Cu^{II}_6L_{24}(H_2O)_4Br_4]Br_8$ (**2**), $[Fe^{III}_8Cu^{II}_6L_{24}(H_2O)_{10}](NO_3)_{12}$ (**3**), $[Fe^{III}_8Ni^{II}_6L_{24}(SCN)_{11}Cl]$ (**4**) and $[Fe^{III}_8Co^{II}_6L_{24}(SCN)_{10}(H_2O)_2]Cl_2$ (**5**). The metallic skeleton of each cage describes a cube in which the Fe^{III} ions occupy the eight vertices and the M^{II} ions lie at the center of the six faces. Direct current (DC) magnetic susceptibility and magnetization measurements on **3** - **5** reveal the presence of weak antiferromagnetic exchange between the metal ions in all three cases. Computational techniques known in theoretical nuclear physics as statistical spectroscopy, which exploit the moments of the Hamiltonian to calculate relevant thermodynamic properties, determine $J_{Fe\text{-}Cu} = 0.10$ cm^{-1} for **3** and $J_{Fe\text{-}Ni} = 0.025$ cm^{-1} for **4**. Q-band EPR spectra of **1** reveal a significantly wider spectral width in comparison to $[FeL_3]$, indicating that the magnitude of the Fe^{III} zero-field splitting (ZFS) is larger in the heterometallic cage than in the monomer.

INTRODUCTION

Polymetallic cages of Fe^{III} have long played a prominent role in the field of molecule-based magnets, often producing aesthetically pleasing complexes possessing fascinating magnetic properties.[1] In 1992 an $[Fe_{19}]$ cage was reported whose structure is related to goethite, $\{Fe(O)OH\}_n$, and whose synthesis hinted at the processes underpinning the formation of naturally occurring iron oxo-hydroxo species.[2] In 2004 an even simpler hydrolysis methodology was employed to produce an $[Fe_{17}]$ cage that is a structural analogue of the mineral magnetite.[3] Both $[Fe_{19}]$ and $[Fe_{17}]$ possess large spin ground states of $S \simeq 33/2$ and $S = 35/2$, respectively. Another structurally related species, a fluoride-based $[Fe_{13}]$ cage reported in 2002, represented the first example of an open-shell Keggin ion. Like $[Fe_{19}]$ and $[Fe_{17}]$, competing anitferromagnetic exchange interactions in $[Fe_{13}]$ stabilize a non-zero ground state spin value.[4] The first Fe^{III} based Single-Molecule Magnet (SMM) was a tacn-based (1,4,7-triazacyclononane) $[Fe_8]$ complex possessing an anisotropic $S = 10$ ground state,[5] later followed by a family of $[Fe_4]$ complexes with a star-like topology and $S = 5$ ground states, originating from antiferromagnetic exchange between the central ion and its three neighbors.[6]

Large, isotropic, spin ground states are key to certain species demonstrating an enhanced magnetocaloric effect (MCE) that can be exploited for low temperature magnetic refrigeration, and the first Fe^{III} cage to show promise in this regard was a high symmetry $[Fe_{14}]$ cluster based on a hexacapped hexagonal bipyramid, with $S = 25$.[7] Iron rings of various sizes, most, if not all, characterized by antiferromagnetic exchange and diamagnetic spin ground states, have proved invaluable for the investigation of quantum size effects. For example, the archetypal $[Fe_{10}]$ 'ferric wheel' displays stepped magnetization at very low temperatures indicative of field-induced excited state level crossings.[8] Perhaps the Fe^{III} cluster that has garnered the most attention is the $[Fe_{30}]$ icosidodecahedron embedded in a Mo-based polyoxometalate (POM).[9] Indeed a search of the literature reveals an astonishing 84 papers devoted to just this one molecule; the interest arising from geometric spin frustration, a phenomenon akin to that observed in extended materials such as the Kagome lattice.[10] More recently even larger nuclearity Fe^{III} species have been reported – including a cyanide-bridged $[Fe_{42}]$ cage displaying ferromagnetic exchange and a $S = 45$ ground state, a tetrahedral $[Fe_{60}]$ cluster whose building blocks are the $[Fe_4]$ star-shaped SMMs, and an $[Fe_{64}]$ cubic complex incorporating both formate and triethanolamine.[11,12]

We recently began a project focussed on the modular construction of large transition metal cages based on the self-assembly of simple metallosupramolecular building blocks. While not a new approach for the construction of cages of paramagnetic metal ions, it is a somewhat under-exploited methodology.[13] Our initial investigations have examined the metalloligand $[M^{III}L_3]$ (HL = 1-(4-pyridyl)butane-1,3-dione), which

features a tris(acac) octahedral transition metal core functionalized with three *para*-pyridyl donor groups (Figure 1).[14,15] ^{1}H NMR spectroscopy of the diamagnetic $[Al^{III}L_3]$ species shows that it exists as a mixture of the *mer* and *fac* configurations in solution, with the self-assembly process amplifying the proportion of the *fac*-configuration during cage formation.[15] Thus $[M^{III}L_3]$ can be regarded as a simple tritopic donor with the N-atoms of the pyridyl rings disposed at 90° with respect to each other. We previously showed that the combination of the *fac*–isomer of $[Cr^{III}L_3]$ with square-planar M^{II} connectors leads to the formation of $[Cr^{III}_8M^{II}_6]^{12+}$ (M^{II} = Ni, Co) molecular cubes,[14] and herein we extend this study to the synthesis, structures and magnetic properties of the Fe^{III}-based cages $[Fe^{III}_8Pd^{II}_6L_{24}]Cl_{12}$ (**1**), $[Fe^{III}_8Cu^{II}_6L_{24}(H_2O)_4Br_4]Br_8$ (**2**), $[Fe^{III}_8Cu^{II}_6L_{24}(H_2O)_{10}](NO_3)_{12}$ (**3**), $[Fe^{III}_8Ni^{II}_6L_{24}(SCN)_{11}Cl]$ (**4**) and $[Fe^{III}_8Co^{II}_6L_{24}(SCN)_{10}(H_2O)_2]Cl_2$ (**5**).

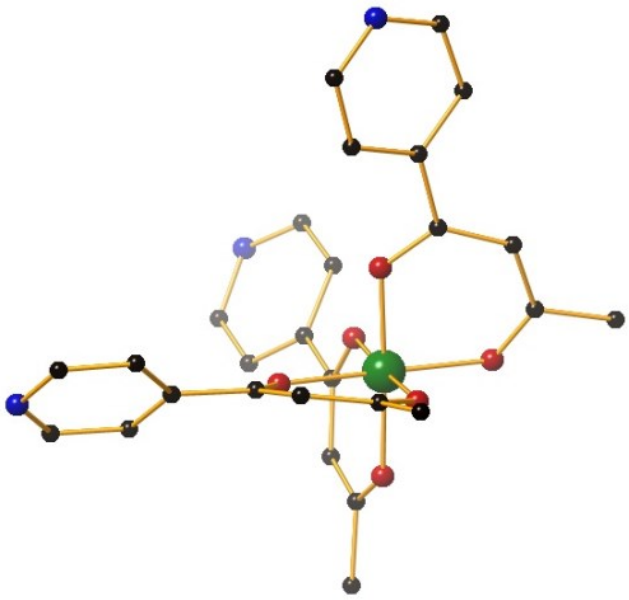

Figure 1. The molecular structure of the *fac*-configuration of the $[M^{III}L_3]$ metalloligand. Colour code: M^{III} = green, O = red, N = blue, C = black. H-atoms omitted for clarity.

EXPERIMENTAL SECTION

Syntheses

$[Fe^{III}L_3]$. $FeCl_3$ (1 mmol, 162 mg), 1-(4-pyridyl)butane-1,3-dione (3.5 mmol, 570 g) and NaOMe (3.5 mmol, 189 mg) were dissolved in MeOH/H_2O (1:1, 25 mL) and left to stir until a red product precipitated (~24 h). The precipitate was filtered and washed with water. The crude product was extracted with CH_2Cl_2 and dried over anhydrous $MgSO_4$. The CH_2Cl_2 was removed under reduced pressure to afford the product as a red solid. Yield (0.46 g, 85 %). Elemental analysis (%) calculated (found) for $C_{27}H_{24}N_3O_6Fe$ (542.34): C 59.79 (59.53), H 4.46 (4.39), N 7.75 (7.67).

$[Fe^{III}_8Pd^{II}_6L_{24}]Cl_{12}$ (1). A solution of $AgNO_3$ (0.16 mmol, 28 mg,) and $[Pd(benzonitrile)_2Cl_2]$ (0.08 mmol, 32 mg) in $CHCl_3$/MeOH (1:1, 10 mL) was stirred for 30 minutes at room temperature. The solution was then filtered, added to a solution of $[Fe^{III}L_3]$ (0.055 mmol, 30 mg) in 10 mL of MeOH, and allowed to stand. Dark-red crystals (87 % yield, 32 mg) suitable for single crystal X-ray diffraction were obtained by slow evaporation of the mother liquor after 3 days. Elemental analysis (%) calculated (found) for $C_{216}H_{192}N_{24}O_{48}Cl_{12}Fe_8Pd_6$ (5402.67): C 48.02 (48.31), H 3.58 (3.31), N 6.22 (6.12).

$[Fe^{III}_8Cu^{II}_6L_{24}(H_2O)_4Br_4]Br_8$ (2). $[Fe^{III}L_3]$ (0.2 mmol, 108 mg) in CH_2Cl_2 (10 mL) was added to a solution of $CuBr_2$ (0.2 mmol, 45 mg) in MeOH (10 mL). The mixture was stirred for 3 hours before being filtered. Black crystals (48 %, 69 mg) suitable for single crystal X-ray diffraction were formed from slow evaporation of the mother liquor after two days. Elemental analysis (%) calculated (found) for $C_{216}H_{200}N_{24}O_{52}Br_{12}Fe_8Cu_6$ (5750.98): C 45.11 (45.01), H 3.51 (3.24) N 5.85 (6.04).

$[Fe^{III}_8Cu^{II}_6L_{24}(H_2O)_{10}](NO_3)_{12}$ (3). $[Fe^{III}L_3]$ (0.1 mmol, 54 mg), $Cu(NO_3)_2{\cdot}3H_2O$ (0.1 mmol, 24 mg,) and pyrazine (0.4 mmol, 32 mg) were dissolved in a solution of CH_2Cl_2/EtOH (1:1, 20 mL). The reaction mixture was stirred for 3 hours at room temperature, before being filtered and allowed to stand. Red crystals (65 % yield, 46 mg) suitable for single crystal X-ray diffraction were obtained from slow evaporation of the mother liquor after 2 days. Elemental analysis (%) calculated (found) for $C_{216}H_{212}N_{36}O_{94}Fe_8Cu_6$ (5644.21): C 45.96 (45.49), H 3.79 (3.68), N 8.93 (8.54).

$[Fe^{III}_8Ni^{II}_6L_{24}(SCN_{11})Cl]$ (4). $NiCl_2$ (0.2 mmol, 26 mg) and $[Fe^{III}L_3]$ (0.2 mmol, 108 mg) were stirred in a mixture of CH_2Cl_2/MeOH (1:1, 20 mL). After 20 minutes KSCN (0.4 mmol, 39 mg) dissolved in H_2O (2 mL) was added to the reaction mixture, which was allowed to stir for a further 30 minutes before being filtered. Red crystals (71 % yield, 95 mg) suitable for single crystal X-ray diffraction were obtained from slow evaporation of the mother liquor after 4 days. Elemental analysis (%) calculated (found) for $C_{227}H_{192}N_{35}O_{48}S_{11}ClFe_8Ni_6$ (5365.24): C 50.82 (50.13), H 3.61 (3.70), N 9.14 (9.27).

$[Fe^{III}_8Co^{II}_6L_{24}(SCN)_{10}(H_2O)_2]Cl_2$ (5). $CoCl_2$ (0.2 mmol, 26 mg) and $[Fe^{III}L_3]$ (0.2 mmol, 108 mg) were stirred in a mixture of CH_2Cl_2/MeOH (1:1, 20 mL). After 20 minutes KSCN (0.4 mmol, 39 mg) dissolved in H_2O (2 mL) was added to the reaction mixture, which was left to stir for a further 30 minutes. The solution was then filtered and allowed to stand. Red crystals (62 % yield, 83 mg) suitable for single crystal X-ray diffraction were obtained from slow evaporation of the mother liquor after 3 days. Elemental analysis (%) calculated (found) for $C_{226}H_{196}N_{34}O_{50}S_{10}Cl_2Fe_8Co_6$ (5380.08): C 50.45 (50.81), H 3.67 (3.70), N 8.85 (9.21).

Crystal structure information

For compounds **1**, **2**, **4**, **5** and **$[Fe^{III}L_3]$** single-crystal X-ray diffraction data were collected at T = 100 K on a Rigaku AFC12 goniometer equipped with an enhanced sensitivity (HG) Saturn 724+ detector mounted at the window of a FR-E+ Superbright MoKα (λ = 0.71075 Å) rotating anode generator with HF Varimax optics (100 μm focus)[16] using Rigaku Crystal Clear and CrysalisPro software[17,18] for data collection and reduction. Due to very weak scattering power, single-crystal X-ray diffraction data for **3** were collected at T = 30.15 K using a synchrotron source (λ = 0.6889 Å) on the I19 beam line at Diamond Light Source on an undulator insertion device with a combination of

double crystal monochromator, vertical and horizontal focussing mirrors and a series of beam slits. The same software as above was used for data refinement. Unit cell parameters in all cases were refined against all data. Crystals of all samples were very sensitive to solvent loss, and so to minimize crystal degradation and maintain crystalline uniformity, crystals of all six compounds were 'cold mounted' on MiTeGen Micromounts™ at *ca*. T = 203 - 223 K using Sigma-Aldrich fomblin Y® LVAC (3300 mol. wt.) with the X-Temp 2[19] crystal cooling system attached to the microscope. The crystal structures of **[$Fe^{III}L_3$]** and **5** were solved using the charge flipping method implemented in SUPERFLIP,[20] whereas **1** ,**2**, **3** and **4** were solved using intrinsic phasing methods as implemented in SHELXT.[21] All structures were refined on F_o^2 by full-matrix least-squares refinements using ShelXL[22] within the OLEX2 suite.[23] All non-hydrogen atoms were refined with anisotropic displacement parameters, and all hydrogen atoms were added at calculated positions and refined using a riding model with isotropic displacement parameters based on the equivalent isotropic displacement parameter (U_{eq}) of the parent atom. All crystal structures (except **[$Fe^{III}L_3$]**) contain large accessible voids and channels that are filled with diffuse electron density belonging to uncoordinated solvent, whose electron contribution was accounted for by the SQUEEZE[24] solvent masking routine as implemented in PLATON software.[25]To maintain reasonable molecular geometry, DFIX/DANG restraints were used in **2**, **3** and **4**, whereas SIMU, DELU, RIGU and ISOR restraints were applied to model appropriately atomic displacement parameters (ADP). For heavily disordered atoms EADP constraints were also applied.

Crystal data for [$Fe^{III}L_3$] $C_{27}H_{30}N_3O_{10}Fe$, M = 612.39, trigonal, a = b = 14.8322(3) Å, c = 7.5892(3) Å, α = β =90.0 °, γ = 120.0 °, V = 1445.89(9) Å^3, Z = 2, *P-3*, D_c = 1.407 g/cm^3, μ = 0.581 mm^{-1}, T = 100 K, λ = 0.71075 Å, 27014 reflections collected, 2665 independent reflections (R_{int}= 0.0626), Final R indices [$F^2 > 2\sigma(F^2)$] = 0.0419, R indices (all data) = 0.0496. CCDC 1522561.

Crystal data for 1 $C_{216}H_{206}N_{24}O_{54}Cl_4Fe_8Pd_6$, M = 5229.04, orthorhombic, a = 30.4249(5) Å, b = 31.3338(4) Å, c = 38.6462(5) Å, α = β = γ = 90.0 °, V = 36842.5(9) Å^3, Z = 4, *Pcca*, D_c = 0.943 g/cm^3, μ = 0.669 mm^{-1}, T = 100 K, λ = 0.71075 Å, 191457 reflections collected, 42250 independent reflections (R_{int}= 0.0780), Final R indices [$F^2 > 2\sigma(F^2)$] = 0.0688, R indices (all data)= 0.1159. CCDC 1522562.

Crystal data for 2 $C_{216}H_{200}N_{24}O_{52}Br_4Fe_8Cu_6$, M = 5111.67, tetragonal, a = 20.076(3) Å, b = 20.076(3) Å, c = 37.225(3) Å, α = β = γ = 90.0 °, V = 15.003(5) Å^3, Z = 2, *P4/nnc*, D_c = 1.131 g/cm^3, μ = 1.383 mm^{-1}, T = 100 K, λ = 0.71075 Å, 74790 reflections collected, 6640 independent reflections (R_{int}= 0.1258), Final R indices [$F^2 > 2\sigma(F^2)$] = 0.0845, R indices (all data) = 0.1217. CCDC 1522563.

Crystal data for 3 $C_{216}H_{210}N_{24}O_{58}Fe_8Cu_6$, M = 4898.11, orthorhombic, a = 29.6051(6) Å, b = 31.3962(4) Å, c = 38.0783(6) Å, α = β = γ = 90.0 °, V = 35393.3(10) Å^3, Z = 4, *Pcca*, D_c = 0.919 g/cm^3, μ = 0.667 mm^{-1}, T = 30 K, λ = 0.6889 Å, 282293 reflections collected, 31228 independent reflections (R_{int}= 0.2011), Final R indices [$F^2 > 2\sigma(F^2)$] = 0.1121, R indices (all data) = 0.1587. CCDC 1522564.

Crystal data for 4 $C_{227}H_{192}N_{35}O_{48}S_{11}ClFe_8Ni_6$, M = 5365.31, tetragonal, a = 29.644(12) Å, b = 29.644(12) Å, c = 26.851(10) Å, α = β = γ = 90.0 °, V = 23596(21) Å^3, Z = 2, *P4/n*, D_c = 0.755 g/cm^3, μ = 0.567 mm^{-1}, T = 100 K, λ = 0.71075 Å, 89872 reflections collected, 20990 independent reflections (R_{int}= 0.0863), Final R indices [$F^2 > 2\sigma(F^2)$] = 0.1003, R indices (all data) = 0.1331. CCDC 1522565.

Crystal data for 5 $C_{230}H_{200}N_{34}O_{50}S_{10}Cl_{10}Fe_8Co_6$, M = 5715.71, tetragonal, a = 29.5218(3) Å, b = 29.5218(3) Å, c = 26.6262(5) Å, α = β = γ = 90.0 °, V = 23205.8(7) Å^3, Z = 2, *P4/n*, D_c = 0.818 g/cm^3, μ = 0.596 mm^{-1}, T = 100 K, λ = 0.71075 Å, 119893 reflections collected, 20470 independent reflections (R_{int}= 0.0382), Final R indices [$F^2 > 2\sigma(F^2)$]= 0.0743, R indices (all data)= 0.1002. CCDC 1522566.

RESULTS AND DISCUSSION

Structure Description: The metallic skeleton common to **1-5** describes a $[Fe^{III}{}_8M^{II}{}_6]^{12+}$ cube with the Fe^{III} ions occupying the eight corners and the M^{II} ions (Pd, Co, Ni, Cu) situated slightly above (1.2-1.5 Å) the center of the square faces (Figures 2-3, Figure S1). The dimensions of the cube are of the order Fe···Fe ≃ 12 Å^3, with $Fe^{III}\cdots M^{II}$ ≃ 9 Å. The Fe^{III} ions are six-coordinate and in distorted {FeO_6} octahedral geometries with Fe–O distances between 1.93–2.04 Å, and *cis*/*trans* angles in the range 85.4–96.8° and 170.8–176.6°, respectively. The [$Fe^{III}L_3$] moieties each coordinate to three different M^{II} ions through the N-atoms of their pyridyl rings, with M^{II}-N distances in the range 1.97–2.17 Å. In turn, each M^{II} ion is equatorially coordinated to four different [$Fe^{III}L_3$] units.

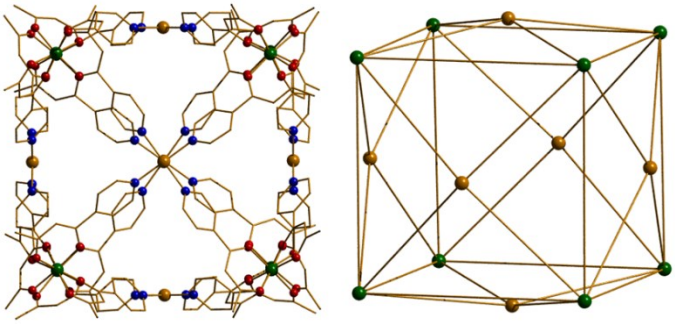

Figure 2. Molecular structure (left) and metallic skeleton (right) of complex **1**. Colour code: Fe = green, Pd = orange, N = blue, O = red, C = gold. H-atoms omitted for clarity.

The Pd ions in compound **1** display square planar geometry with Pd-N distances of ~2 Å and Pd^{II}-N *cis*/*trans* angles ~90°/180° (Figure 2). The remaining compounds display higher coordination numbers at the M^{II} sites, all being square pyramidal or octahedral in geometry – the apical sites being occupied by the anions present in the starting materials ($CuBr_2$ (**2**), $Cu(NO_3)_2{\cdot}3H_2O$ (**3**), $Co(SCN)_2$ (**5**)), the KSCN (**4**) added to the reaction mixture, and/or solvent/H_2O molecules. However, these sites are, in some cases, severely disordered. See the SI for further discussion.

Structures **1-5** (Figures 2-3, Figure S1) crystallize as homochiral racemates - that is as enantiomeric mixtures in which all eight [$Fe^{III}L_3$] moieties in a single cube possess either Δ or Λ stereochemistry. Although this could be a packing effect, which results in selective crystallization from a more complex diastereomeric mixture, homochiral assemblies are frequently observed to be energetically preferred in solution.[26] Volume calculations performed on **1-5** using the ^{3}V Volume Assessor program show internal cavities sizes of ≤ 1300 Å^3.[27]

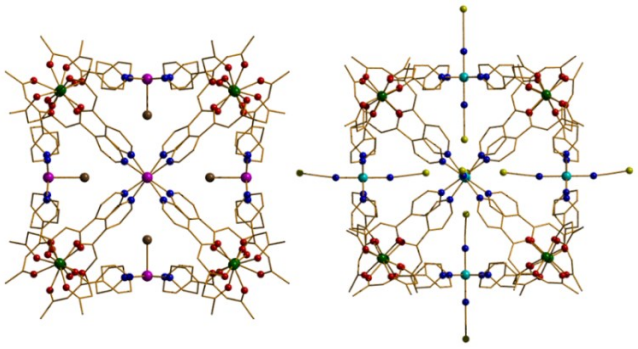

Figure 3. Molecular structures of compounds **2** (left) and **4** (right). Colour code as in Figure 2. Cu = pink, Ni = light blue, Br = brown, S = yellow. H-atoms and counter ions omitted for clarity.

SQUID Magnetometry: The direct current (DC) molar magnetic susceptibility, χ, of polycrystalline samples of complexes **3 - 5** were measured in an applied magnetic field, *B*, of 0.1 T, over the 5–290 K temperature, *T*, range (Figure 4, where χ = *M*/*B*, and *M* is the magnetization). Because of loss of lattice solvent, during the evacuation of the sample chamber of the SQUID magnetometer, leading to uncertainty in the molar mass of the measured sample, the 290 K χ*T* products of **3-5** were scaled to values of 37.25, 41.0 and 46.25 cm^3 mol^{-1} K, respectively. These values are those expected from the spin-only contributions to the magnetism of an [$Fe^{III}_8Cu^{II}_6$] unit (37.25 cm^{3}mol^{-1}K), with g_{Fe}=2.00 and g_{Cu}=2.00, of an [$Fe^{III}_8Ni^{II}_6$] unit (41.0 cm^{3}mol^{-1}K), with g_{Fe}=g_{Ni}=2.00, and of an [$Fe^{III}_8Co^{II}_6$] unit (46.25 cm^{3}mol^{-1}K), with g_{Fe}=g_{Co}=2.00, where g_{Fe}, g_{Cu}, g_{Ni}, and g_{Co} are the *g*-factors of Fe^{III}, Cu^{II}, Ni^{II}, and Co^{II}, respectively. The rescaled values presented maximum deviations of the order of 15 % from the unscaled values. Upon cooling, the χ*T* products of **3** and **4** remain essentially constant down to 50 K, below which a rapid decrease is observed in both cases. For **5** the deviation from Curie law begins around at 180 K, falling steadily to a value of ~42 cm^3 K mol^{-1} at *T* = 15 K, before decreasing much more abruptly below this temperature. In each case, the behavior is indicative of weak antiferromagnetic exchange interactions between the metal ions, with the added effect of moderate-large zero-field splitting (ZFS, Ni^{II}, Co^{II}) in the case of **4** and **5**.

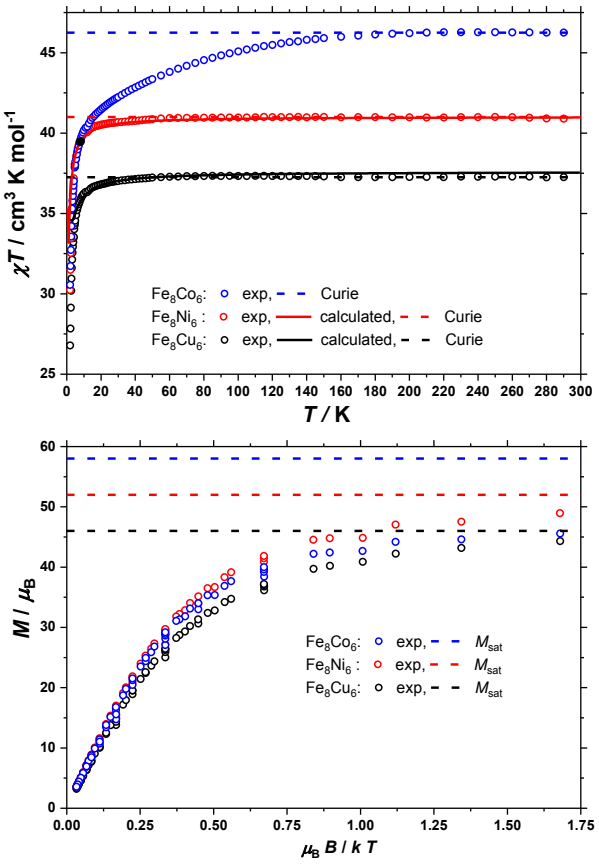

Figure 4. Plot of χ*T* versus *T* for complexes **3-5** measured in an applied field of *B* = 0.1 T (top). The solid lines are a fit of the experimental data. The dashed lines are the Curie constants. Magnetization data for **3-5** measured in the temperature and field ranges, *T* = 2-7 K, *B* = 0-7 T (bottom). The dashed lines indicate the saturation value expected for the field-induced alignment of all isotropic spin centers.

The quantitative interpretation of the magnetic properties of **3-5** based on the diagonalization of a spin-Hamiltonian matrix is impossible since the matrices involved are of dimensions of the order 10^8, 10^9 and 10^{10}, respectively. Even the total spin (*S*) block matrices used in approaches based on Irreducible Tensor Operator algebra are of larger dimension than what is realistic for exact numerical matrix diagonalization. Therefore, to model the magnetic properties of **3-5** we have adapted computational techniques known in theoretical nuclear physics as statistical spectroscopy,[28] which exploit the moments of the Hamiltonian to calculate relevant thermodynamic properties. To describe the magnetic properties of **3-5** we used the following isotropic spin-Hamiltonian (1):

$$\hat{H}_{iso} = J_{\text{Fe-M}} \sum_{\text{all Fe-M pairs}} \hat{S}_{\text{Fe}} \cdot \hat{S}_{\text{M}} + \mu_{\text{B}} B g \sum_{\text{i}} \hat{S}_{\text{i}}^{Z} \qquad (1)$$

with *i* running over all constitutive metal centres, $\hat{S}$ a spin-operator, μ_B the Bohr magneton, *B* the applied magnetic field and *g* the isotropic *g*-factor common to both Fe and M = Cu (**3**), Ni

(**4**) and Co (**5**). We calculate the temperature-dependent magnetic susceptibility of **3** - **5** by use of the Van Vleck equation (2), derived from (1):

$$\chi = \frac{N_A g^2 \mu_B^2}{k_B T} \frac{\sum_S (2S+1) \frac{S(S+1)}{3} \exp(-\frac{E_S}{k_B T})}{\sum_S (2S+1) \exp(-\frac{E_S}{k_B T})} \qquad (2)$$

with N_A Avogadro's number, k_B the Boltzmann constant, and T the temperature. We approximate the energy dependence of the (2S+1) factor in the denominator by a continuous density of states, $\rho_{(E)}$. Similarly, we approximate the energy dependence of the (2S+1)S(S+1)/3 factor on the nominator, by a continuous density, $C_{(E)}$, which we designate the Curie-constant density. Thus:

$$\chi = \frac{N_A g^2 \mu_B^2}{k_B T} \frac{\sum_S C_{(E)} \rho_{(E)} \exp(-\frac{E_S}{k_B T})}{\sum_S \rho_{(E)} \exp(-\frac{E_S}{k_B T})} \qquad (3)$$

These two densities, $C_{(E)}$ and $\rho_{(E)}$, may be obtained from moments of an appropriate Hamiltonian,[29] here (1). The moments are related to the traces of powers of the Hamiltonian.[29] The density $\rho_{(E)}$ is determined from the moments of a Hamiltonian containing only the Heisenberg terms of (1), whereas the density $C_{(E)}$ is determined from the bivariate moments of (1), *i.e.* those obtained from a Hamiltonian containing both Heisenberg and Zeeman terms. Once these moments, up to order 14 in our case, have been computed, the densities are conveniently determined following the method described in the literature.[30,31] Using this approach, and by successive simulations of the temperature dependence of the χT product of **3**- **4**, we determine $J_{Fe\text{-}Cu}$ = 0.10 cm^{-1} with a common isotropic g-factor g_1 = 2.0 for **3**, and $J_{Fe\text{-}Ni}$ = 0.025 cm^{-1} with a common isotropic g-factor g_2 = 2.0 for **4**. Note that J in each case is of the same order of magnitude as D_{Fe} and likely much smaller than D_{Ni} (see the EPR section below).

Magnetization measurements performed on **3**-**5** in the T = 2-7 K and B = 0-7 T temperature and field ranges are shown in the lower panel of Figure 4. The data for **3** saturate at the value expected for the field-induced alignment of the spins on the constituent metal centers (46 μ_B), while that of **4** and **5** are below their expected saturation values, consistent with the presence of significant D_{Ni} and D_{Co} in this temperature regime.

EPR Spectroscopy: We previously reported EPR spectra of [FeL$_3$], which gave the ZFS of the Fe^{III}, s = 5/2 ion as $|D|$ = 0.08 cm^{-1} with rhombicity of $|E/D| \approx 1/3$.[15] The rhombic nature of the ZFS is consistent with reports on simple Fe^{III} tris-diketonates, although D is slightly smaller: [Fe(acac)$_3$] ($|D|$ = 0.16 cm^{-1}, E/D = 0.3) and [Fe(dpm)$_3$] (dpm = dipivaloylmethane; D = -0.20 cm^{-1}, $|E/D|$ = 0.25).[32] Q-band EPR spectra of **1**, where M = Pd^{II} is diamagnetic, reveal a significantly wider spectral width *cf.* [FeL$_3$] (Figure 5), indicating that the magnitude of the Fe^{III} ZFS is larger in {Fe$_8$M$_6$} than in the monomer. Note that the distortions of the [FeO$_6$] octahedra in the latter are slightly bigger than the former, and are also somewhat larger than that seen for the [CrO$_6$] octahedra in the analogous Cr-based cubes reported in ref [14].The relatively poor spectral resolution limits the accuracy of the determination of the ZFS parameters. Crude simulations give $|D|$ *ca*. 0.17 cm^{-1} with $|E/D|$ again close to 1/3 (from trial calculations $|E/D| > 0.3$). Spectra of **2**-**4** are similar to those of **1** and, within the limits imposed by the poor resolution, show no direct evidence of either spectral features of the M^{II} = Cu or Ni ions nor of any weak exchange effects beyond further broadening. Hence, from the EPR of these materials we are restricted to concluding that there is a small absolute increase in $|D|$ in going from [FeL$_3$] to {Fe$_8$M$_6$}. This was also true for {Fe$^{III}_2$M$^{II}_3$} trigonal bipyramidal complexes built with the same metalloligand, reported previously,[14d] where we found similar values of D_{Fe} *ca*. 0.20 cm^{-1} (also fully rhombic).

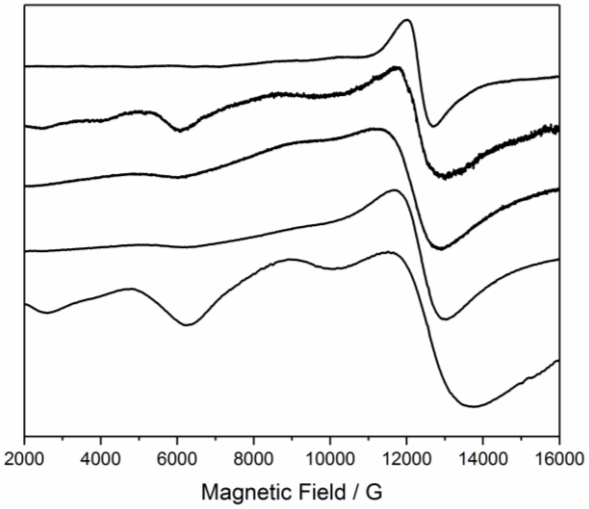

Figure 5. Q-band EPR spectra of powdered samples of (from top to bottom) **[FeL$_3$]**, **1**, **2**, **3** and **4** at 5 K.

We previously noted that incorporation of [CrL$_3$] ($|D|$ = 0.55 cm^{-1}) into {Cr$^{III}_2$M$^{II}_3$} led to an increase in $|D_{Cr}|$ from 0.55 cm^{-1} to 0.61 and 0.64 cm^{-1} for M = Zn and Pd, respectively (these gave much better resolved EPR spectra and D could be determined more accurately). This is an increase of ~10-15% in D. The Fe systems seem more sensitive, with a *ca*. 100% increase in D (although a similar absolute increase of *ca*. 0.1 cm^{-1}). Previous angular overlap model studies on Fe^{III} tris-diketonates showed D to be very sensitive to the trigonal distortion at Fe^{III}.[6b] This may also be the cause for the much greater broadening in the EPR spectra of the Fe complexes than their Cr analogues: the sensitivity of the ZFS parameters to small variations in the coordination geometry make the spectra much more susceptible to strain effects.

CONCLUSIONS

The mononuclear complex [Fe^{III}L$_3$] (HL = 1-(4-pyridyl)butane-1,3-dione), which features a tris(acac) octahedral transition metal core functionalized with three *para*-pyridyl donor groups, can be regarded as a simple tritopic donor

that can be employed as a building block for the construction of polymetallic cage compounds. Reaction with a variety of different M^{II} salts produces a family of heterometallic $[Fe^{III}_8Pd^{II}]^{12+}$ (**1**), $[Fe^{III}_8Cu^{II}_6]^{8+}$ (**2**), $[Fe^{III}_8Cu^{II}_6]^{12+}$ (**3**), $[Fe^{III}_8Ni^{II}_6]$ (**4**) and $[Fe^{III}_8Co^{II}_6]^{2+}$ (**5**) cubes in which the Fe^{III} ions occupy the eight vertices and the M^{II} ions lie at the center of the six faces. Magnetic susceptibility measurements reveal weak antiferromagnetic exchange between the paramagnetic metal ions in **3**-**5**. The quantitative interpretation of the magnetic properties for such large species based on the diagonalization of a spin-Hamiltonian matrix is impossible, since the matrices involved are of enormous dimensions. In order to overcome this problem computational techniques known as statistical spectroscopy were employed. This afforded $J_{Fe\text{-}Cu} = 0.10$ cm^{-1} for **3** and $J_{Fe\text{-}Ni} = 0.025$ cm^{-1} for **4**. Q-band EPR spectra of $[Fe^{III}_8Pd^{II}_6L_{24}]Cl_{12}$ revealed a significantly wider spectral width in comparison to the monomeric $[FeL_3]$ species, indicating that the magnitude of the Fe^{III} ZFS is larger in $\{Fe_8M_6\}$ than in the monomer.

ASSOCIATED CONTENT

Supporting Information

The associated Supporting Information includes notes on the crystallographic disorder at the apical sites of the M^{II} ions, figures of complexes **2** and **5**, and packing diagrams of all complexes highlighting the extended structure in the crystal. The Supporting Information is available free of charge on the ACS Publications website (Supporting Information.pdf). CIF Files have been deposited with the Cambridge Structural Database (https://www.ccdc.cam.ac.uk) and can be retrieved using the identifiers listed for each compound.

AUTHOR INFORMATION

Corresponding Author

*E.Brechin@ed.ac.uk
*piligkos@chem.ku.dk
*Paul.Lusby@ed.ac.uk
*S.Calvo@ed.ac.uk

ORCID ID

Euan Brechin: 0000-0002-9365-370X
Stergios Piligkos: 0000-0002-4011-6476
Paul Lusby: 0000-0001-8418-5687
Sergio Sanz: 0000-0002-4790-4184
Helen O'Connor: 0000-0003-0044-2469
Mateusz Pitak: 0000-0002-3680-7100
Simon Coles: 0000-0001-8414-9272
Høgni Weihe: 0000-0001-6194-1486
Eric McInnes: 0000-0002-4090-7040
Nick Chilton: 0000-0002-8604-0171

Notes

The authors declare no competing financial interest.

ACKNOWLEDGMENT

EKB and PJL thank the EPSRC for funding (EP/P025986/1 & EP/N01331X/1). EKB also thanks the Velux Foundations for a Villum Visiting Professor Programme Grant. We thank the EPSRC for funding the UK National Crystallography service and the UK National EPR Facility. We would like to acknowledge Diamond Light Source for time on beamline I-19 (proposal MT11238-2).

REFERENCES

(1) Gatteschi, D.; Sessoli, R.; Cornia, A. Single-molecule magnets based on iron(III)oxo clusters. *Chem. Commun*, **2000**, 725-732.

(2) (a) Heath, S. L.; Powell, A. K The Trapping of Iron Hydroxide Units by the Ligand "heidi": Two New Hydroxo(oxo)iron Clusters Containing 19 and 17 Iron Atoms. *Angew. Chem. Int. Ed. Engl.* **1992**, *31*, 191-193. (b) Powell, A. K.; Heath, S. L.; Gatteschi, D.; Pardi, L.; Sessoli, R.; Spina, G.; Del Giallo, F.; Pieralli, F. Synthesis, Structures, and Magnetic Properties of Fe2, Fe17, and Fe19 Oxo-Bridged Iron Clusters: The Stabilization of High Ground State Spins by Cluster Aggregates. *J. Am. Chem. Soc*., **1995**, *117*, 2491-2501.

(3) (a) Powell, G. W.; Lancashire, H. N.; Brechin, E. K.; Collison, D.; Heath, S. L.; Mallah, T.; Wernsdorfer, W. Building Molecular Minerals: All Ferric Pieces of Molecular Magnetite. *Angew. Chem. Int. Ed.* **2004**, *43*, 5772-5775. (b) Vecchini, C.; Ryan, D. H.; Cranswick, L. M. D.; Evangelisti, M.; Kockelmann, W.; Radaelli, P. G.; Candini, A.; Affronte, M.; Gass, I. A.; Brechin, E. K.; Moze, O. From single-molecule magnetism to long-range ferromagnetism in $Hpyr[Fe_{17}O_{16}(OH)_{12}(py)_{12}Br_4]Br_4$. *Phys. Rev. B*. **2008**, *77*, 224403.

(4) (a) Bino, A.; Ardon, M.; Lee, D.; Spingler, B.; Lippard, S. J. Synthesis and Structure of $[Fe_{13}O_4F_{24}(OMe)_{12}]^{5-}$: The First Open-Shell Keggin Ion. *J. Am. Chem. Soc*. **2002**, *124*, 4578-4579. (b) van Slageren, J.; Rosa, P.; Caneschi, A.; Sessoli, R.; Casellas, H.; Rakitin, Y. V.; Cianchi, L.; Del Giallo, F.; Spina, G.; Bino, A.; Barra, A.-L.; Guidi, T.; Carretta, S.; Caciuffo, R. Static and dynamic magnetic properties of an $[Fe_{13}]$ cluster. *Phys. Rev. B*. **2006**, *73*, 014422.

(5) (a) Delfs, C.; Gatteschi, D.; Pardi, L.; Sessoli, R.; Wieghardt, K.; Hanke, D. Magnetic properties of an octanuclear iron(III) cation. *Inorg. Chem*. **1993**, *32*, 3099-3103; (b) Wieghardt, K.; Pohl, K.; Jibril, I.; Huttner, G. Hydrolysis Products of the Monomeric Amine Complex $(C_6H_{15}N_3)FeCl_3$: The Structure of the Octameric Iron(III) Cation of $\{[(C_6H_{15}N_3)_6Fe_8(\mu_3\text{-}O)_2(\mu_2\text{-}OH)_{12}]Br_7(H_2O)\}Br\cdot 8H_2O$. *Angew. Chem. Int. Ed. Engl*. **1984**, *24*, 77-78.

(6) (a) Moragues-Cánovas, M.; Rivière, E.; Ricard, L.; Paulsen, C.; Wernsdorfer, W.; Rajaraman, G.; Brechin, E. K.; Mallah, T. Resonant Quantum Tunneling in a New Tetranuclear Iron(III)-Based Single-Molecule Magnet. *Adv. Mater.* **2004**, *16*, 1101-1105. (b) Barra, A. L.; Caneschi, A.; Cornia, A.; Fabrizi de Biani, F.; Gatteschi, D.; Sangregorio, C.; Sessoli, R.; Sorace, L. Single-Molecule Magnet Behavior of a Tetranuclear Iron(III) Complex. The Origin of Slow Magnetic Relaxation in Iron(III) Clusters. *J. Am. Chem. Soc*. **1999**, *121*, 5302-5310.

(7) (a) Low, D. M.; Jones, L. F.; Bell, A.; Brechin, E. K.; Mallah, T.; Rivière, E.; Teat, S. J.; McInnes, E. J. L. Solvothermal Synthesis of a Tetradecametallic Fe^{III} Cluster *Angew. Chem. Int. Ed*. **2003**, *42*, 3781-3784. (b) Evangelisti, M.; Candini, A.; Ghirri, A.; Affronte, M.; Brechin, E. K.; McInnes, E. J. L. Spin-enhanced magnetocaloric effect in molecular nanomagnets. *Appl. Phys. Lett.* **2005**, *87*, 072504.

(8) Taft, K. L.; Delfs, C. D.; Papaefthymiou, G. C.; Foner, S.; Gatteschi, D.; Lippard. S. J. $[Fe(OMe)_2(O_2CCH_2Cl)]_{10}$, a Molecular Ferric Wheel. J. *Am. Chem. Soc*. **1994**, *116*, 823-832.

(9) Garlea, V. O.; Nagler, S. E.; Zarestky, J. L.; Stassis, C.; Vaknin, D.; Kögerler, P.; McMorrow, D. F.; Niedermayer, C.; Tennant, D. A.; Lake, B.; Qiu, Y.; Exler, M.; Schnack, J.; Luban, M. Probing spin frustration in high-symmetry magnetic nanomolecules by inelastic neutron scattering. *Phys. Rev. B*. **2006**, *73*, 024414.

(10) Schnack, J. Effects of frustration on magnetic molecules: a survey from Olivier Kahn until today. *Dalton Trans*. **2010**, *39*, 4677-4686.

(11) Kang, S.; Zheng, H.; Liu, T.; Hamachi, K.; Kanegawa, S.; Sugimoto, K.; Shiota, Y.; Hayami, S.; Mito, M.; Nakamura, T.; Nakano, M.; Baker, M. L.; Nojiri, H.; Yoshizawa, K.; Duan, C.; Sato,

O. A ferromagnetically coupled Fe_{42} cyanide-bridged nanocage. *Nat. Commun*. **2015**, *6*, 5955.

(12) (a) Jiménez, J.-R.; Mondal, A.; Chamoreau, L.-M.; Fertey, P.; Tuna, F.; Julve, M.; Bousseksou, A.; Lescouëzec, R.; Lisnard, L. An $\{Fe_{60}\}$ tetrahedral cage: building nanoscopic molecular assemblies through cyanometallate and alkoxo linkers. *Dalton Trans*. **2016**, 45, 17610-17615. (b) Liu, T.; Zhang, Y.-J.; Wang, Z.-M.; Gao, S. A 64-Nuclear Cubic Cage Incorporating Propeller-like Fe^{III}_8 Apices and $HCOO^-$ Edges. *J. Am. Chem. Soc*. **2008**, *130*, 10500-10501.

(13) (a) Castellano, M.; Ruiz-García, R.; Cano, J.; Ferrando-Soria, J.; Pardo, E.; Fortea-Pérez, F. R.; Stiriba, S.-E.; Barros, W. P.; Stumpf, H. O.; Cañadillas-Delgado, L.; Pasán, J.; Ruiz-Pérez, C.; de Munno, G.; Armentano, D.; Journaux, Y.; Lloret, F.; Julve, M. Metallosupramolecular approach toward multifunctional magnetic devices for molecular spintronics. *Coord. Chem. Rev.* **2015**, *303*, 110-138. (b) Rebilly, J.-N.; Mallah, T. *Struct. Bonding* (Berlin), **2006**, *122*, 103-131; (c) Aromí, G.; Aguilà, D.; Gamez, P.; Luis, F.; Roubeau, O. Design of magnetic coordination complexes for quantum computing. *Chem. Soc. Rev*. **2012**, *41*, 537-546; (d) Andruh, M. Compartmental Schiff-base ligands—a rich library of tectons in designing magnetic and luminescent materials. *Chem. Commun*. **2011**, *47*, 3025-3042.

(14) (a) Wu, H.-B.; Wang, Q.-M. Construction of Heterometallic Cages with Tripodal Metalloligands. *Angew. Chem. Int. Ed*. **2009**, 48, 7343-7345; (b) Sanz, S.; O'Connor, H. M.; Moreno Pineda, E.; Pedersen, K. S.; Nichol, G. S.; Mønsted, O.; Weihe, H.; Piligkos, S.; McInnes, E. J. L.; Lusby, P. J.; Brechin, E. K. $[Cr^{III}_8M^{II}_6]^{12+}$ Coordination Cubes (M^{II}=Cu, Co). *Angew. Chem. Int. Ed*. **2015**, *54*, 6761-6764; (c) O'Connor, H. M.; Sanz, S.; Pitak, M. B.; Coles, S. J.; Nichol, G. S.; Piligkos, S.; Lusby, P. J.; Brechin, E. K. $[Cr^{III}_8M^{II}_6]^{n+}$ (M^{II} = Cu, Co) face-centred, metallosupramolecular cubes. *CrystEngComm*. **2016**, *18*, 4914-4920; (d) Sanz, S.; O'Connor, H. M.; Martí-Centelles, V.; Comar, P.; Pitak, M. B.; Coles, S. J.; Nichol, G. S.; Palacios, E.; Evangelisti, M.; Baldansuren, A.; Chilton, N. F.; McInnes, E. J. L.; Weihe, H.; Piligkos, S.; Lusby, P. J.; Brechin, E. K. $[M^{III}_2M^{II}_3]^{n+}$ trigonal bipyramidal cages based on diamagnetic and paramagnetic metalloligands. *Chem. Sci.* **2017**, *8*, 5526-5535.

(15) For other examples of heterobimetallic cages, see: (a) Sun, S.-S.; Stern, C. L.; Nguyen, S. T.; Hupp, J. T. Directed Assembly of Transition-Metal-Coordinated Molecular Loops and Squares from Salen-Type Components. Examples of Metalation-Controlled Structural Conversion. *J. Am. Chem. Soc*. **2004**, 126, 6314-6326; (b) Hiraoka, S.; Sakata, Y.; Shionoya, M. Ti(IV)-Centered Dynamic Interconversion between Pd(II), Ti(IV)-Containing Ring and Cage Molecules. *J. Am. Chem. Soc*. **2008**, 130, 10058–10059; (c) Li, H.; Han, Y.-F,; Lin, Y.-J.; Guo, Z.-W.; Jin, G.-X. Stepwise Construction of Discrete Heterometallic Coordination Cages Based on Self-Sorting Strategy. *J. Am. Chem. Soc*. **2014**, 136, 2982−2985; (d) Li, F.; Clegg, J. K.; Jensen, P.; Fisher, K.; Lindoy, L. F.; Meehan, G. V.; Moubaraki, B.; Murray, K. S. Predesigned Hexanuclear Cu^{II} and Cu^{II}/Ni^{II} Metallacycles Featuring Six-Node Metallacoronand Structural Motifs. *Angew. Chem. Int. Ed*. **2009**, 48, 7059 –7063; (e) Ramsay, W. J.; Rizzuto, F. J.; Ronson, T. K.; Caprice, K.; Nitschke, J. R. Subtle Ligand Modification Inverts Guest Binding Hierarchy in $M^{II}_8L_6$ Supramolecular Cubes. *J. Am. Chem. Soc*. **2016**, 138, 7264−7267; (f) Bar, A. K.; Chakrabarty, T.; Mostafa, G.; Mukherjee, P. S. Self-Assembly of a Nanoscopic $Pt_{12}Fe_{12}$ Heterometallic Open Molecular Box Containing Six Porphyrin Walls. *Angew. Chem. Int. Ed*. **2008**, 47, 8455 –8459; (g) Schultz, A.; Li, X.; Barkakaty, B.; Moorefield, C, N.; Wesdemiotis, C.; Newkome, G. R. Stoichiometric Self-Assembly of Isomeric, Shape-Persistent, Supramacromolecular Bowtie and Butterfly Structures. *J. Am. Chem. Soc*. **2012**, 134, 7672−7675; (h) Mahata, K.; Saha, M. L.; Schmittel, M. From an Eight-Component Self-Sorting Algorithm to a Trisheterometallic Scalene Triangle. J. Am. Chem. Soc. **2010**, 132, 15933–15935l; (i) Smulders, M. M. J.; Jiménez, A. Nitschke, J. R. *Angew. Chem. Int. Ed*. **2012**, 51, 6681–6685.

(16) Coles, S. J.; Gale, P. A. Changing and challenging times for service crystallography. *Chem. Sci*. **2012**, *3*, 683–689.

(17) Rigaku Oxford Diffraction, in CrystalClear-SM Expert 3.1 b27, **2012**.

(18) Rigaku Oxford Diffraction, in CrysAlisPro 1.171.38.41, **2015**.

(19) Kottke, T.; Stalke, D. Crystal handling at low temperatures. *J. Appl. Crystallogr*. **1993**, *26*, 615-619.

(20) Palatinus, L.; Chapuis, G. SUPERFLIP – a computer program for the solution of crystal structures by charge flipping in arbitrary dimensions *J. Appl. Crystallogr*. **2007**, *40*, 786–790.

(21) Sheldrick, G. M. SHELXT - Integrated space-group and crystal-structure determination. *Acta Cryst*. **2015**, A71, 3-8.

(22) Sheldrick, G. M. Crystal structure refinement with SHELXL. *Acta Crystallogr. Sect. A Found. Crystallogr*. **2015**, *c71*, 3-8.

(23) Dolomanov, O. V.; Blake, A. J.; Champness, N. R.; M. Schröder, M. OLEX: new software for visualization and analysis of extended crystal structures. *J. Appl. Crystallogr*. **2003**, *36*, 1283-1284.

(24) Spek, A. L. PLATON SQUEEZE: a tool for the calculation of the disordered solvent contribution to the calculated structure factors. *Acta Cryst*. **2015**, C71, 9-18.

(25) Spek, A. L. Structure validation in chemical crystallography. *Acta Cryst*. **2009**, D65, 148-155

(26) Castilla, A. M.; Ramsay, W. J.; Nitschke, J. R. Stereochemistry in Subcomponent Self-Assembly. *Acc. Chem. Res*. **2014**, *47*, 2063-2073.

(27) Voss, N. R.; Gerstein, M. 3V: cavity, channel and cleft volume calculator and extractor. *Nucleic Acids Res*. **2010**, *38*, W555-W562.

(28) Wong, S. S. M. Nuclear Statistical Spectroscopy, Oxford University Press and Clarendon Press, Oxford, **1986**.

(29) Rushbrooke, G. S.; Wood, P. J. On the Curie points and high temperature susceptibilities of Heisenberg model ferromagnetics. *Mol. Phys*. **1958**, *1*, 257-283.

(30) (a) Mead, L. R.; Papanicoaou, N. Maximum entropy in the problem of moments. *J. Math. Phys*. **1984**, 25, 2404-2417. (b) Grimes, S. M.; Massey, T. N. Inclusion of two-body effects in calculating nuclear level densities. *Fusion Eng. Des*. **1997**, *37*, 89-93.

(31) Grimes, S. M.; Massey, T. N. New expansion technique for spectral distribution calculations. *Phys. Rev. C.* **1995**, *51*, 606-610.

(32) Collison, D.; Powell, A. K. Electron spin resonance studies of "FeO6" tris chelate complexes: models for the effects of zero-field splitting in distorted S = 5/2 spin systems. *Inorg. Chem.* 1990, 29, 4735-4746.

TOC Graphic:

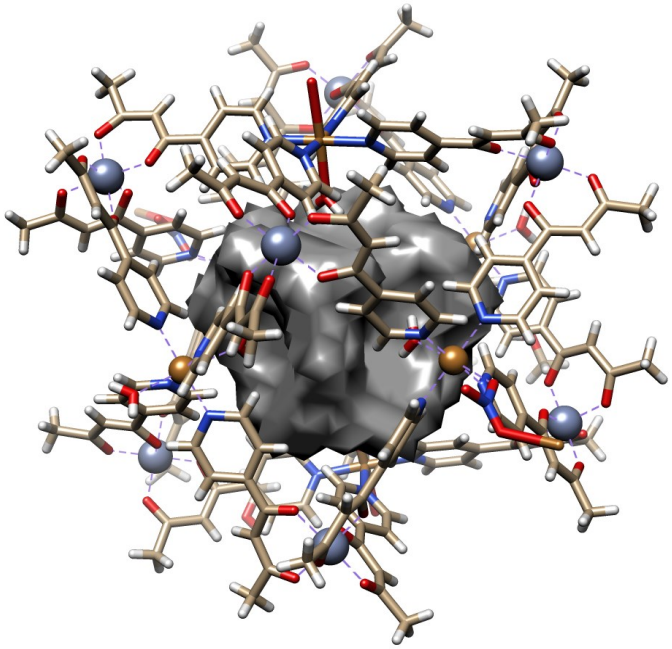

TOC Synopsis: Five heterometallic $[Fe^{III}_8M^{II}_6]^{n+}$ cages (M^{II} = Pd, Co, Ni, Cu) are constructed from the self-assembly of the metalloligand $[Fe^{III}L_3]$ (HL = 1-(4-pyridyl)butane-1,3-dione) with a variety of M^{II} salts.